Supporting Information

Zero-field-cooling exchange bias up to room temperature in the strained kagome antiferromagnet $Mn_{3.1}Sn_{0.9}$

Mingyue Zhao,[a] Wei Guo,[a] Xian Wu,[a] Li Ma,[*a] Ping Song,[*b] Guoke Li,[a] Congmian Zhen,[a] Dewei Zhao,[a] and Denglu Hou[a]

Affiliations

[a]Hebei Key Laboratory of Photophysics Research and Application, College of Physics, Hebei Normal University, Shijiazhuang, 050024, People's Republic of China

[b]State Key Laboratory of Metastable Materials Science &Technology and Key Laboratory for Microstructural Material Physics of Hebei Province, School of Science, Yanshan University, Qinhuangdao 066004, People's Republic of China
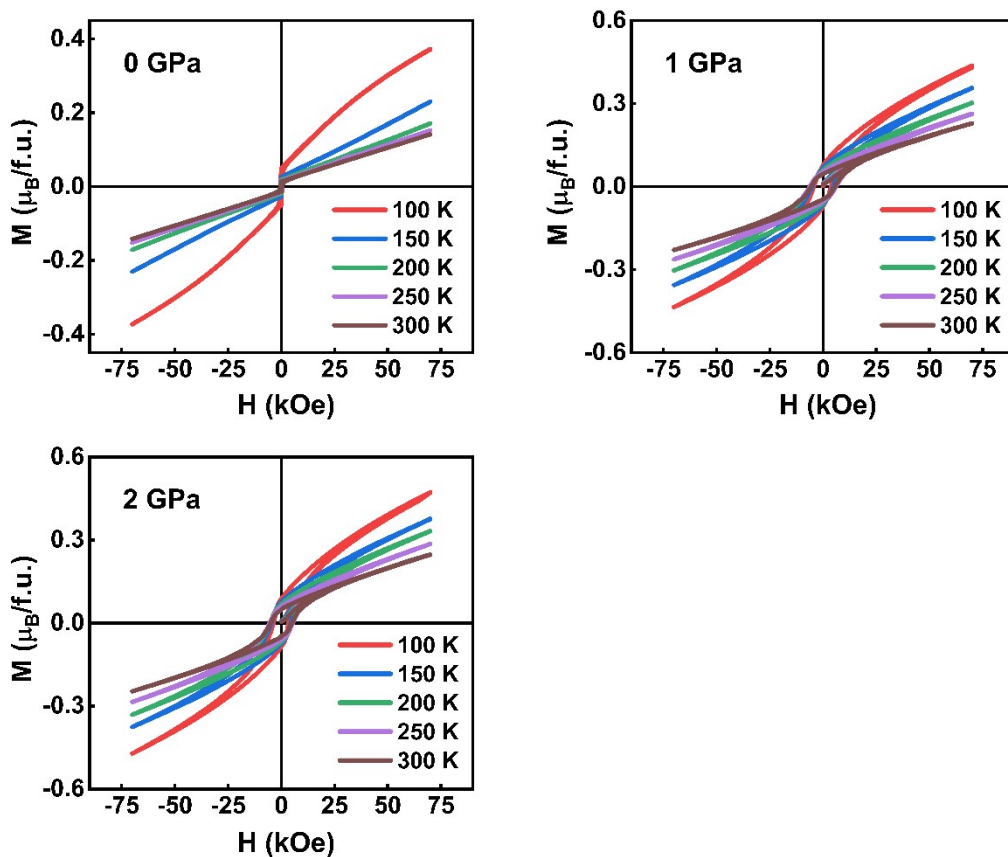
Experimental details

Fig. S1. Magnetic hysteresis loops at different temperatures under zero-field cold conditions for $Mn_{3.1}Sn_{0.9}$ after undergoing uniaxial compressive stress deformations of 0 GPa, 1 GPa and 2 GPa, respectively.
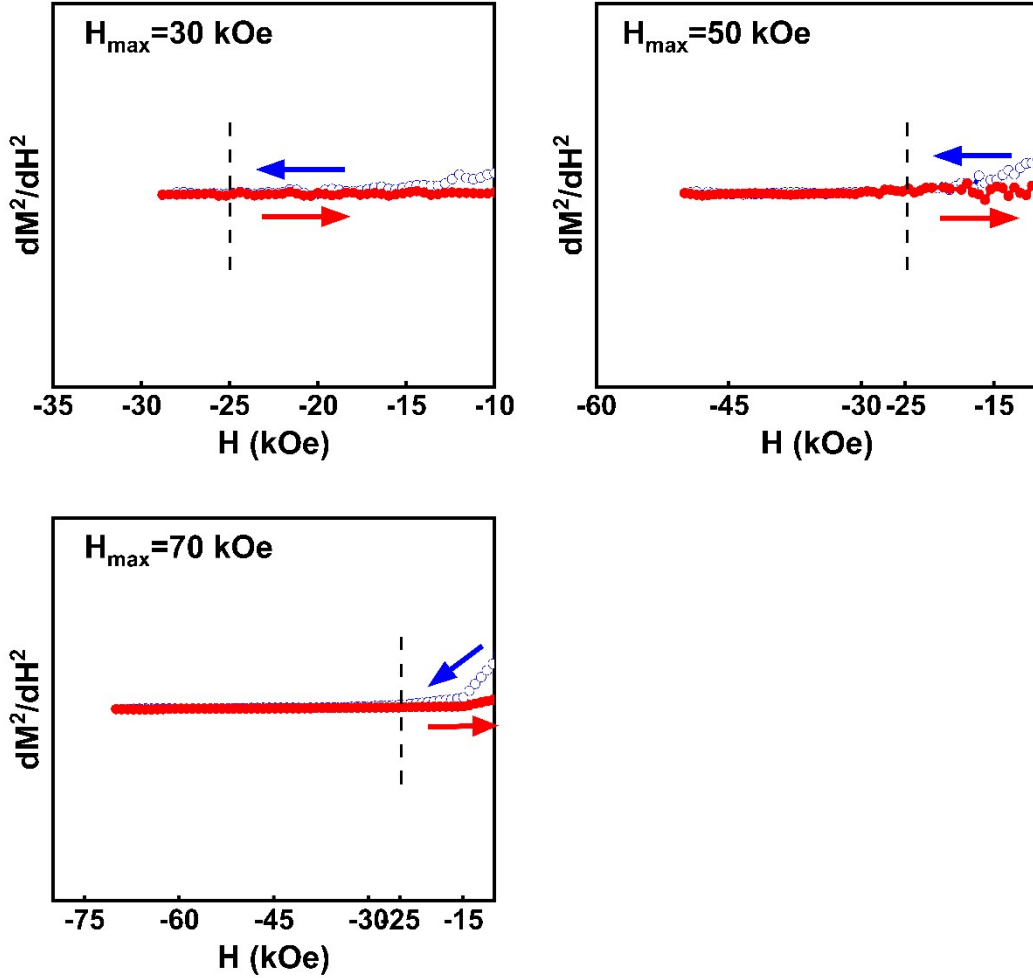

Fig. S2. The second derivatives of the 1 GPa ZFC loops measured with different the maximum applied fields H_{max} from 30 kOe to 70 kOe at 100 K (the ascending branches are in red full circles and the descending branches are in blue hollow circles). For better visualization, only the field regions of interest are plotted.

Fig. S2 shows the d^2M/dH^2 of the ZFC loops in high field regions (negative) measured with different H_{max}. All of the ascending branches overlap the descending branches at the similar field value about 25 kOe. According to the Singular Point Detection (SPD) method,[1, 2] the anisotropy field (H_A) may around 25 kOe. Therefore, we can infer that the $M(H)$ curves of 1 GPa measured between the H_{max} above 25 kOe can be a major loop.
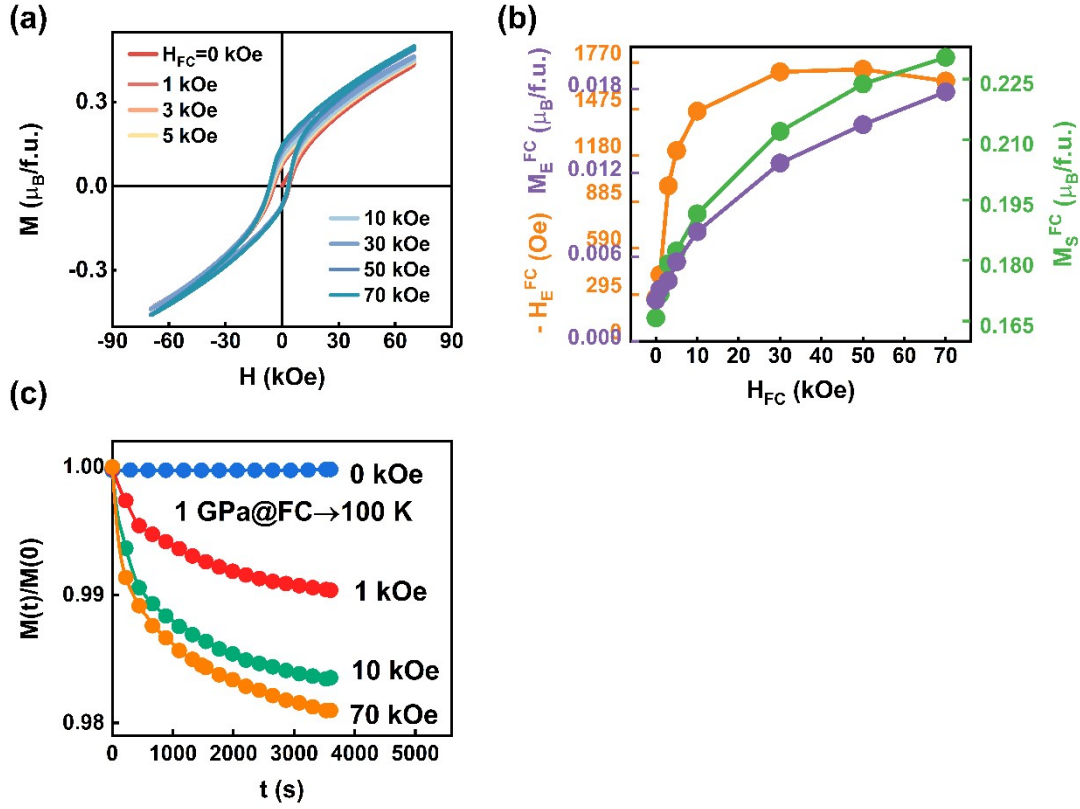
Fig. S3. (a) Hysteresis loops measured at 100 K after different cooling fields H_{FC} for the 1 GPa sample, and (b) the corresponding horizonal shift H_E^{FC} vertical shift M_E^{FC} and spontaneous magnetization M_S^{FC} as a function of H_{FC}. (c) Time dependence of the normalized magnetization at 100 K at 500 Oe for $Mn_{3.1}Sn_{0.9}$ after undergoing a stress deformation of 1 GPa and exposure to different cooling fields. See text for all specific protocols prior to each magnetic relaxation measurement.

Fig. S3(a) shows the hysteresis loops at 100 K for the 1 GPa sample under different cooling fields. Fig. S3(b) shows the changes of H_E^{FC}, M_E^{FC} and M_S^{FC} calculated from Fig. S3(a) with the H_{FC} of the cooling field. The quantitative feedback shows that H_E^{FC}, M_E^{FC} and M_S^{FC} are all it increases with the increase of H_{FC}. Fig. S3(c) shows the time dependence of the normalized magnetization at 100 K at 500 Oe for the 1 GPa sample after undergoing different cooling fields to further reflect the effect of the cooling field on the uncompensated AFM state. The 1 GPa sample was cooled to 100 K under a cooling field of 0 kOe, 1 kOe, 10 kOe, or 70 kOe before measurement. It can be seen that there is no relaxation phenomenon in the system under zero cooling field. Moreover, with the increase of cooling field, the relaxation phenomenon is sharply enhanced. Therefore, the cooling field not only determines the presence or absence of magnetic relaxation, but also controls the strength of magnetic relaxation. The above information shows that in addition to the applied field, the cooling field can also induce the magnetic transition from the stable noncollinear AFM state to the uncompensated AFM state, bringing about a pinning phase for exchange bias that ultimately leads to its ability to control the values of H_E^{FC} and M_E^{FC}.
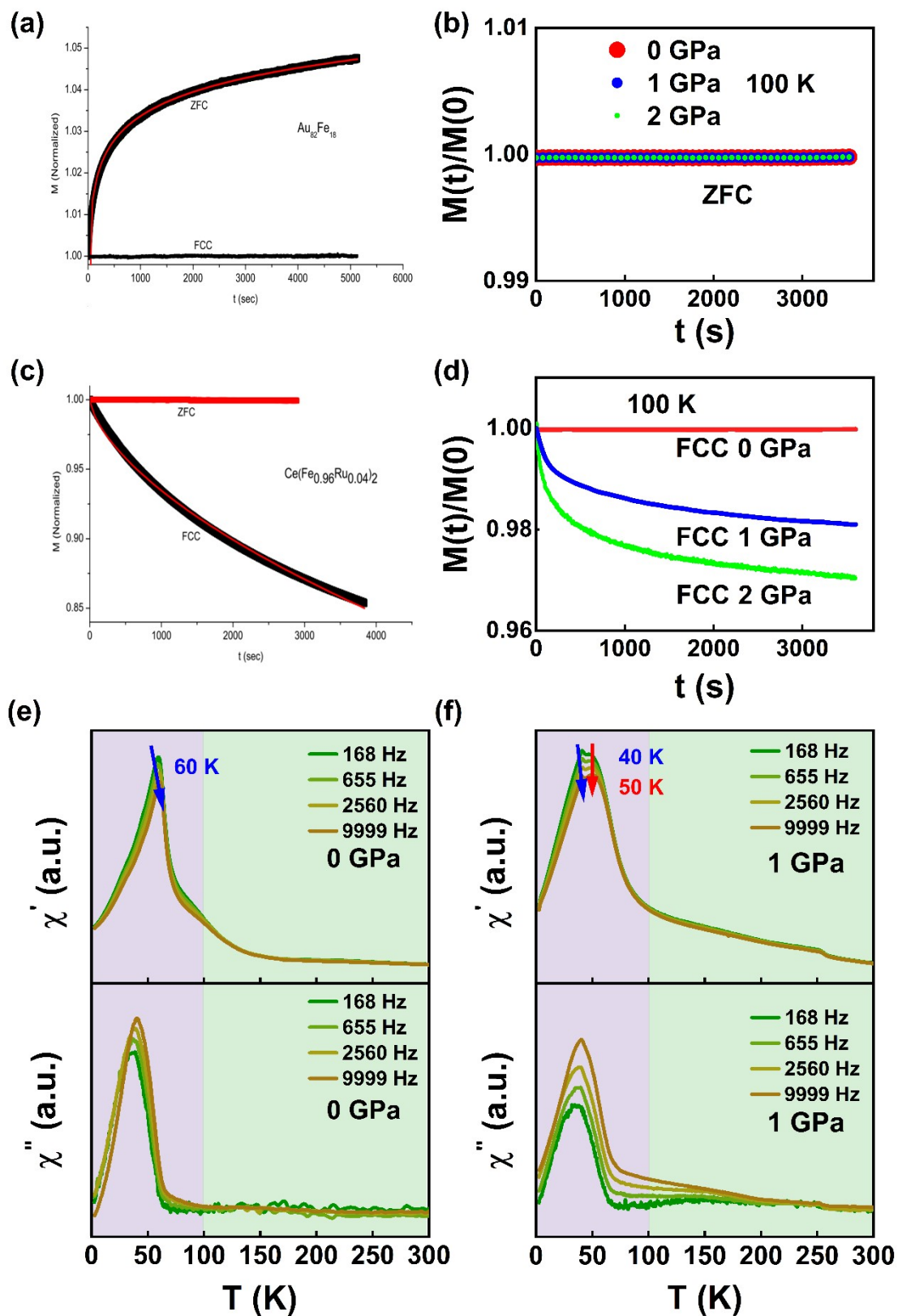
Fig. S4. Exclusion of spin glass in stress-deformed $Mn_{3.1}Sn_{0.9}$ at 100 K and confirmation of magnetic glass. (a) Time dependence of normalized magnetization for

Au$_{82}$Fe$_{18}$ at $T = 14$ K (spin glass) obtained under ZFC and FCC protocols from reference 3. (b) Time dependence of normalized magnetization for 0 GPa, 1 GPa, and 2 GPa samples at $T = 100$ K obtained under ZFC protocol. (c) Time dependence of normalized magnetization for Ce(Fe$_{0.96}$Ru$_{0.04}$)$_2$ at $T = 18$ K (magnetic glass) obtained under ZFC and FCC protocols from reference 3. (d) Time dependence of normalized magnetization for 0 GPa, 1 GPa, and 2 GPa samples at $T = 100$ K obtained under FCC protocol. The temperature dependence of the AC susceptibility of the 0 GPa sample (e) and the 1 GPa sample (f) at different frequencies.

In order to distinguish spin glass and magnetic glass, magnetic relaxation and AC susceptibility are measured. According to reference 3, the magnetic relaxation at $T = 100$ K and $H = 500$ Oe under zero field cooling (ZFC) and field cooling (FCC) protocols were measured as shown in Fig. S4. For the 0 GPa sample, both the ZFC and FCC states show no relaxation in magnetization, indicating neither spin glass nor magnetic glass. For the 1 GPa and 2 GPa samples, the ZFC state shows no relaxation in magnetization, while the FCC state shows strong relaxation. These behaviours are consistent with the characteristics of magnetic glass, but not with spin glass. In addition, according to AC susceptibility, the freezing temperature of the spin glass for the 1 GPa sample is 40 K, which is much lower than 100 K. Therefore, both AC susceptibility and magnetic relaxation results show that spin glass does not exist, but magnetic glass does in the stress-deformed Mn$_{3.1}$Sn$_{0.9}$ samples above 100 K. In addition, the AC susceptibility χ' curve for the 0 GPa sample displayed in Fig. S4(e) exhibits a frequency-dependent shoulder near 75 K above (but reasonably close to) the spin glass freezing temperature $T_f = 60$ K. Since the spin glass phase usually influences the system's magnetization at temperatures higher than T_f, the χ'' curve has also been displayed. The χ'' curve for the 0 GPa sample does not show any frequency-dependent shoulder/peak above 75 K, thus the possibility of trace of glassy magnetism above 75 K is unambiguously ruled out.
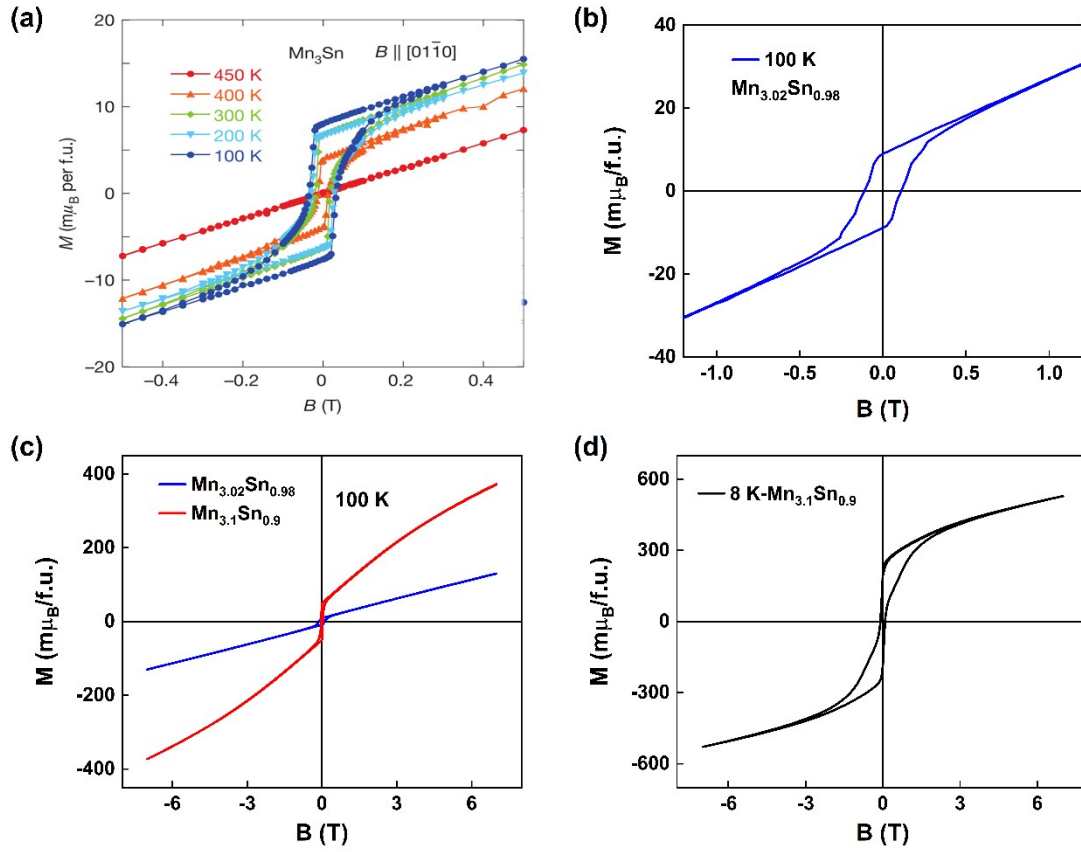
Fig. S5. The magnetic hysteresis loops for $Mn_{3.02}Sn_{0.98}$ single crystal from reference 4 (a) and our measured $Mn_{3.02}Sn_{0.98}$ polycrystal (b). (c) The magnetic hysteresis loops at 100 K for nearly stoichiometric $Mn_{3.02}Sn_{0.98}$ polycrystal (blue curve) and Mn-rich $Mn_{3.1}Sn_{0.9}$ polycrystal (red curve). (d) The magnetic hysteresis loops at 8 K for nearly stoichiometric $Mn_{3.02}Sn_{0.98}$ polycrystal.

To indirectly detect the magnetic configuration of the Mn atoms occupying Sn sites, we prepared nearly stoichiometric $Mn_{3.02}Sn_{0.98}$ polycrystal and measured its magnetic properties for comparative study with Mn-rich $Mn_{3.1}Sn_{0.9}$ polycrystal without stress-deformation. It was found that the effective net atomic magnetic moment of Mn occupying the Sn site is as high as $\sim 3\ \mu_B$/Mn. This fact supports the collinear ferromagnetic configuration of the Mn atoms occupying Sn sites. Furthermore, in the AC susceptibility shown in Fig. S4, no peak associated with metastable glass magnetism is observed above 100 K, thereby ruling out the existence of glass ferromagnetism above 100 K. However, below the freezing temperature (60 K), we do observe glass ferromagnetism as shown in Fig. S5(d), which is consistent with reference 5.

The specific process of obtaining the magnetic moment of the Mn atoms occupying Sn sites is as follows.

Fig. S5(a) shows the magnetic hysteresis loops for $Mn_{3.02}Sn_{0.98}$ single crystal from reference 4 (a) and our measured $Mn_{3.02}Sn_{0.98}$ polycrystal (b). It can be seen that for

nearly stoichiometric $Mn_{3.02}Sn_{0.98}$, whether it is single crystal or polycrystalline, the shapes of their loops are almost the same. Both exhibit a very weak residual magnetization in the low-field part (7 mμ_B per formula unit for single crystal and 8 mμ_B for polycrystal) and a linear increase with increasing magnetic field in the high-field part. The signal of the very weak residual magnetization originates from the fact that only one of the three Mn spins is parallel to the local easy-axis in the a–b plane, while the other two Mn spins are tilted towards the local easy-axis. The signal of the linear increase arises from the inverse triangular non-collinear antiferromagnetic configuration of Mn_3Sn. Therefore, the total magnetic signal of high field comes from two contributions, which are weak ferromagnetic signal and non-collinear antiferromagnetic signal. Both contributions come from the kagome lattice formed by Mn occupying normal Mn sites.

Fig. S5(c) shows the magnetic hysteresis loops at 100 K for nearly stoichiometric $Mn_{3.02}Sn_{0.98}$ polycrystal (blue curve) and Mn-rich $Mn_{3.1}Sn_{0.9}$ polycrystal (red curve). It can be seen that the magnetism is significantly enhanced after the Mn atoms occupy the Sn sites. The total magnetic signal at 70 kOe high field increases from 130 mμ_B/f.u. to 372 mμ_B/f.u..

For Mn-rich $Mn_{3.1}Sn_{0.9}$, the total magnetic signal comes from three contributions, the first two contributions are both from the Mn atoms occupying the normal Mn sites, and the last contribution is from the Mn atoms occupying the Sn sites. Therefore, we follow the processing method of the Hall signal and obtain the last contribution by subtracting the contributions of the first two from the total signal. That is (372-130)/0.08= $\sim$ 3 mμ_B/Mn.
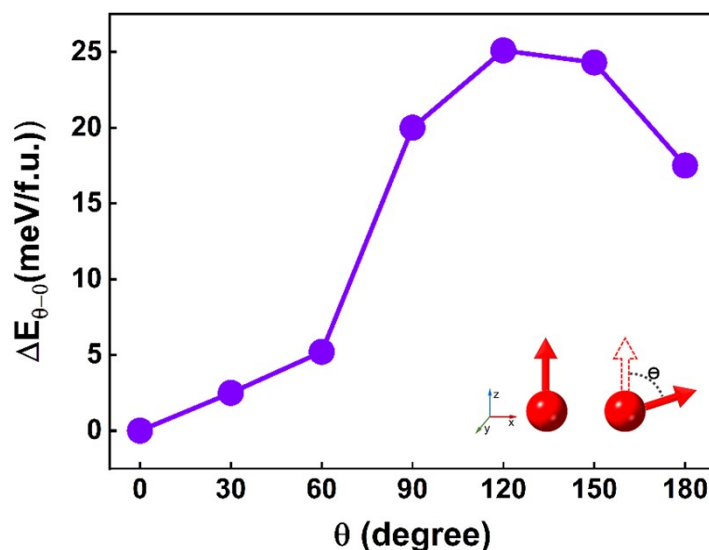
Theoretical details

Fig. S6. The dependence of the energy difference $\Delta E_{\theta-0}$ between the non-collinear magnetic configuration and the collinear FM configuration between Mn atoms occupying Sn sites on θ. The inset is the definition of the angle between the magnetic

moments of the Mn atoms occupying the Sn sites.

The energies of the magnetic configurations of Mn atoms occupying Sn sites were calculated from first-principles. The Mn moments occupying normal Mn sites in $Mn_{3.5}Sn_{0.5}$ have a non-collinear antiferromagnetic configuration, while half of the magnetic moments of the Mn atoms occupying the Sn sites is along the (001) orientation, and the other half are at an angle θ with the (001) orientation. Fig. S6 shows the dependence of the energy difference $\Delta E_{\theta-0}$ between different θ and θ is 0 on θ, where $\Delta E_{\theta-0}$ is defined as $\Delta E_{\theta-0} = E_{\theta} - E_{0}$. The smaller the energy difference, the more stable the corresponding magnetic configuration. As shown in Fig. S6, the most stable magnetic configuration is that the magnetic moment angle between the Mn atoms occupying the Sn sites is 0, indicating that the Mn atoms occupying the Sn sites form a
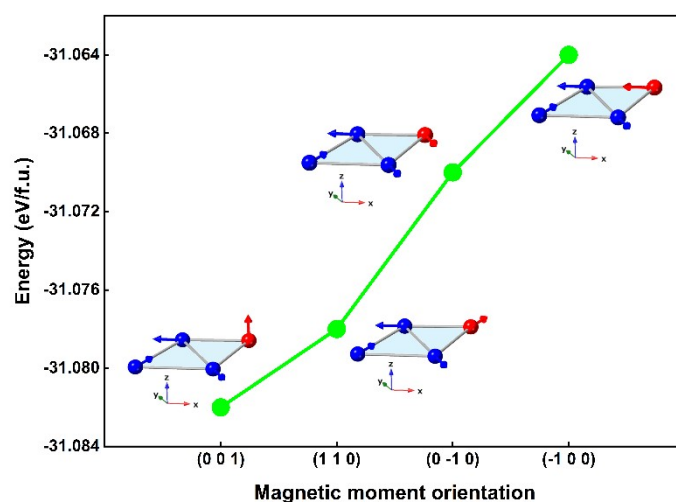
ferromagnetic sublattice.

Fig. S7. Dependence of the energy of the chemical composition of Mn-rich Mn_3Sn on the orientation of the Mn moments occupying Sn sites. The insets are simplified schematic diagrams of the magnetic configuration of the Mn occupying the Sn sites at the corresponding energy. Among them, light blue planes represent kagome lattice planes, blue sphere represent the Mn atoms occupying the normal Mn sites, red sphere represent the Mn atoms occupying the Sn sites, arrow represent magnetic moment.

The Mn atoms occupying the normal Mn sites maintain the non-collinear antiferromagnetic configuration, and the magnetic moments of the Mn atoms occupying the Sn sites are changed to be along the (001), (110), (0-10) and (-100) orientations respectively, so four first-principle calculations were performed, and the calculation results are shown in Fig. S7. The lower the energy, the more stable the corresponding magnetic configuration. The most stable magnetic configuration is that the magnetic moment of the Mn atoms occupying the Sn sites is along the (001)

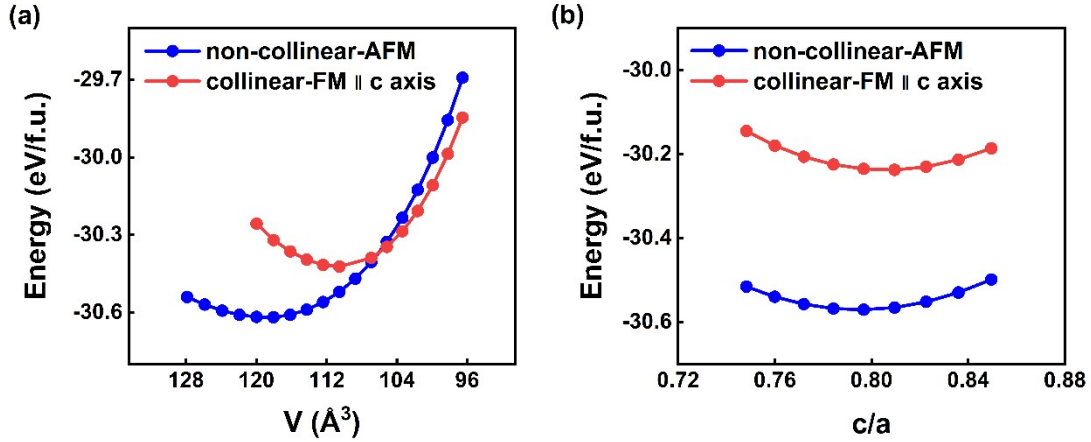orientation, that is, perpendicular to the kagome plane.

Fig. S8. Dependence of energy on the volume of the unit cell V (c) and the crystal axis ratio c/a (d) in the non-collinear AFM configuration (blue curves) and in the collinear FM configuration (red curves), respectively.

In the first set of calculations, the crystal axis ratio c/a was fixed to the experimental value (0.801), and the energy of Mn_3Sn in the two magnetic configurations was calculated under different values of the unit cell volume. Fig. S8(a) shows the dependence of energy on the unit cell volume V in the non-collinear AFM configuration (blue curve) and the collinear FM configuration (red curve). The blue and red curves do not overlap, indicating that the magnetic configuration of the system strongly affects the energy of the system. In particular, the two curves cross at V=106 $Å^3$, which means that the ground state of the system is non-collinear AFM state when the volume is higher than 106 $Å^3$, and the ground state becomes collinear FM state when the volume is lower than 106 $Å^3$. Therefore, the reduction in the volume of the unit cell very helps to stabilize the collinear FM state, as in the case of Mn_3Ge.[6, 7]

In the second set of calculations, the unit cell volume V was fixed to the experimental value (125.37 $Å^3$), and the energy of Mn_3Sn in the two magnetic configurations was calculated under different values of crystal axis ratio c/a. Fig. S8(b) shows the dependence of energy on crystal axis ratio c/a in the non-collinear AFM configuration (blue curve) and in the collinear FM configuration (red curve). The curve of the FM-configured system is always above that of the AFM-configured system, and the two curves have never crossed. This indicates that the magnetic ground state of the system has always been non-collinear AFM for all c/a values in calculations, reflecting that the influence of the crystal axis ratio on the magnetic ground state of the system is much smaller than that of the unit cell volume.

1.	G. Asti and S. Rinaldi, *Phys. Rev. Lett.*, 1972, **28**, 1584-1586.
2.	G. Asti and S. Rinaldi, *J. Appl. Phys.*, 1974, **45**, 3600-3610.
3.	S. B. Roy and M. K. Chattopadhyay, *Phys. Rev. B* 2009, **79**, 052407.
4.	S. Nakatsuji, N. Kiyohara and T. Higo, *Nature*, 2015, **527**, 212–215.
5.	W. J. Feng, D. Li, W. J. Ren, Y. B. Li, W. F. Li, J. Li, Y. Q. Zhang and Z. D. Zhang, *Phys. Rev. B*, 2006, **73**, 205105.
6.	R. D. d. Reis, M. G. Zavareh, M. O. Ajeesh, L. O. Kutelak, A. S. Sukhanov, S. Singh, J. Noky, Y. Sun, J. E. Fischer, K. Manna, C. Felser and M. Nicklas, *Phys. Rev. Mater.*, 2020, **4**, 051401.
7.	A. S. Sukhanov, S. Singh, L. Caron, T. Hansen, A. Hoser, V. Kumar, H. Borrmann, A. Fitch, P. Devi, K. Manna, C. Felser and D. S. Inosov, *Phys. Rev. B*, 2018, **97**, 214402.